Ab initio study of hydrogen in titanium beryllides

D.V. Bachurin, C. Stihl, P.V. Vladimirov

Institute for Applied Materials – Applied Materials Physics, Karlsruhe Institute of Technology,
Hermann-von-Helmholtz-Platz 1, 76344, Eggenstein-Leopoldshafen, Germany

Abstract

Titanium beryllide $Be_{12}Ti$ is a candidate material for the neutron multiplier for the demonstration fusion reactor DEMO. Experimental studies show that under certain conditions, $Be_{12}Ti$ may contain inclusions of other phases such as Be_2Ti, $Be_{17}Ti_2$. In this regard, it is extremely important to study the diffusion of tritium and its isotopes in the crystal lattices of these phases. All calculations are performed using *ab initio* methods. Solution energies of a hydrogen atom in all non-equivalent interstitial sites of the three studied titanium beryllides were found to be lower than that in pure beryllium. The formation energy of all types of vacancies in all studied beryllides is found to be higher than that in beryllium. The binding energies of a single hydrogen atom located both inside and outside the vacancies are calculated. Hydrogen inside monovacancy is more strongly bound as compared to that outside this vacancy. It turned out that in some cases hydrogen can be captured by vacancy being outside of it. The results obtained can be useful for further study of interstitial diffusion of hydrogen and analysis of tritium retention in titanium beryllides.

Keywords: ab initio calculations; titanium beryllides; hydrogen; vacancy; binding energy

Corresponding author: D.V. Bachurin
Email address: dmitry.bachurin@kit.edu

ORCID Ids: D.V. Bachurin: 0000-0001-8995-211X
P.V. Vladimirov: 0000-0003-2358-6043

1. Introduction

The current European Union Demonstration Fusion Power Reactor (EU DEMO) is designed for operation at even more extreme conditions (higher temperatures and stronger irradiation) in contrast to its predecessor the International Thermonuclear Experimental Reactor (ITER). This in turn places high demands on the materials to be used in DEMO. In particular, the modern concept of the helium-cooled pebble bed (HCPB) breeding blanket [1] in ITER implies the use of beryllium pebbles with a diameter of about 1 mm as a functional material for neutron multiplication. However, due to the shortcomings of pure beryllium, which became apparent after post-irradiation examinations, the latter cannot be used in DEMO [2]. Therefore, there is an urgent need for fast screening of advanced materials to select those with superior properties such as high oxidation resistance, low tritium retention, low swelling, high melting point, and overall good compatibility with the structural materials.

Beryllides, i.e., the intermetallic compounds of beryllium with other metals, were proposed as alternative candidates for neutron multiplier material [1]. The synthesis and fabrication processes of beryllides via a combination of plasma sintering and rotating electrode methods were reported in Refs. [3-7]. As an improvement of binary beryllides, ternary compositions of beryllide pebbles [8-11] including surface modification process [12] were proposed.

Currently, beryllides are proposed to be used as a pebble bed [13] or as prismatic hexagonal blocks [14]. The HCPB DEMO tritium-breeding blanket will require ca 400 tons of titanium beryllides. This amount is comparable to the worldwide annual production of beryllium. Fabricating such an amount of neutron multiplier in the form of a pebble bed is challenging and expensive. Therefore, more cost-effective would be the usage of hexagonal blocks, which were recently successfully manufactured by the Ulba Metallurgical Plant (Kazakhstan) and are being investigated at Karlsruhe Institute of Technology [14, 15].

Experimental studies of the phase composition of the $Be_{12}Ti$ compound processed by hot isostatic pressing followed by extrusion demonstrate that, along with the main phase of $Be_{12}Ti$, the structure may contain inclusions of other phases. Namely, Be_2Ti in the form of a thin layer surrounds the pure titanium phase; $Be_{17}Ti_2$ in the form of small particles located at the prior titanium phase locations; pure titanium and beryllium phases, which do not dissolve completely [16, 17]. The data concerning the volume fraction of each of the indicated beryllium phases are not provided in the cited work. It was also shown that some amount of beryllium can evaporate during the fabrication process, thus creating non-stoichiometry, which results in the formation of various phases even if $Be_{12}Ti$ was targeted initially by the powder composition [18, 19]. Thus, during neutron irradiation tritium will be accumulated in all these phases, and during desorption, tritium will inevitably be forced to pass through at least some of the above-mentioned beryllide phases. Therefore, it is very important to study their tritium retention and diffusion for assessing the tritium accumulation after decommissioning of beryllides blocks and/or pebbles from the point of view of operational safety and for subsequent waste management.

In the present work, the behavior of hydrogen in three titanium beryllides (Be_2Ti, $Be_{17}Ti_2$, $Be_{12}Ti$) as well as pure beryllium and titanium are established using *ab initio* methods. In particular, the energy of vacancy formation, hydrogen solution energy, and binding energy of hydrogen with vacancies are calculated, which can be further used for the simulation of hydrogen retention in and release from these materials.

2. Computational technique

2.1. Parameter selection for ab-initio modeling

All calculations are performed using the Vienna Ab-initio Simulation Package (VASP). The results presented in this work are a subset of a larger set of calculations, which is meant to be used as training data for machine learning-based interatomic potentials in future studies. The training data is foreseen to include many different structures containing various other elements in addition to those considered in the present work. Special care is taken to ensure commensurate accuracies of total energies and forces throughout all, current and future, calculations.

To that end, Brillouin-zone sampling is based on the KSPACING parameter and the plane wave basis set is chosen by the energy cut-off as encoded in the ENCUT parameter [20]. When using the KSPACING parameter to handle the Brillouin-zone sampling, $N_i = \lceil max(1, |\vec{b}_i|/KSPACING) \rceil$ *k*-points in the direction of the *i*-th reciprocal lattice vector $\vec{b}_i$ are considered ($i = 1, .., 3$) [21]. In three dimensions, the total amount of *k*-points can therefore be estimated by $N \approx \prod_i N_i \propto KSPACING^{-3} \cdot \prod_i |\vec{b}_i|$, neglecting, in particular, possible reducibility due to symmetries. Thus, the sampling method retains the required property of scaling the considered amounts of *k*-points inversely proportional to the length of each direct lattice vector $|\vec{a}_i|$, while allowing to adjust the overall accuracy by changing the *k*-point grid density for given lattice vectors. In order to obtain roughly equidistant convergence test calculations with grids of approximately N total *k*-points each, KSPACING values distributed according to $KSPACING(N) \propto N^{-\frac{1}{3}}$ between 0.25 and 0.1 with all resulting grids centered at the Γ-point are considered (see the top panel in Fig. 1a for test calculations of pure beryllium). As the wider scope of accumulating training data sets for future studies requires to consider different lattices with commensurate accuracies, the applied measure of accuracy is based on the difference of total energies for the same crystal computed in different unit cells. To that end, calculations of primitive unit cells and, typically tetragonal, conventional unit cells of twice the size are compared for the beryllides. Analogously, for the pure phases, the conventional hexagonal unit cells and an orthorhombic unit cell twice the size are considered, the resulting differences in total energy per atom are shown for beryllium in the middle panel of Fig. 1a. With a KSPACING parameter of about 0.12157, this error is found to be negligible, i.e. about 1.0 meV/atom, for all considered materials. The approximately linear scaling of the resulting numbers of irreducible *k*-points per calculation is illustrated for both unit cells in the bottom panel of Fig. 1a.

Similarly, plane waves with a wave vector $\vec{G}$ are added to the plane wave basis at a *k*-point $\vec{k}$ if $|\vec{G} + \vec{k}| < |\vec{G}_{cut}|$ with $\frac{\hbar^2}{2m}|\vec{G}_{cut}|^2 = ENCUT$ [22]. In three dimensions, this delimits a volume in reciprocal space and circa $N_{plwv} \propto |\vec{G}_{cut}|^3 \propto ENCUT^{\frac{3}{2}}$ plane waves at each *k*-point are expected. For an approximately equidistant sampling, when testing the convergence with respect to ENCUT, values distributed according to $ENCUT(N_{plwv}) \propto {N_{plwv}}^{\frac{2}{3}}$ are considered in the range from 200 to 600 eV as displayed at the top panel of Fig. 1b. However, as future studies comprise helium as well, the basis set needs to accommodate helium with PREC = Accurate as well, introducing the lower bound to ENCUT at 478.896 eV, and thus ENCUT = 486.814 eV is adopted for the present calculations. According to the middle panel of Fig. 1b, it results in a difference of less than 1.0 meV per atom in total energy for beryllium as compared to higher plane wave energy cut-off values. The approximately linear scaling of the minimum, the maximum, and the mean number of considered plane waves at the considered *k*-points are shown for all calculations in the bottom panel of Fig. 1b.

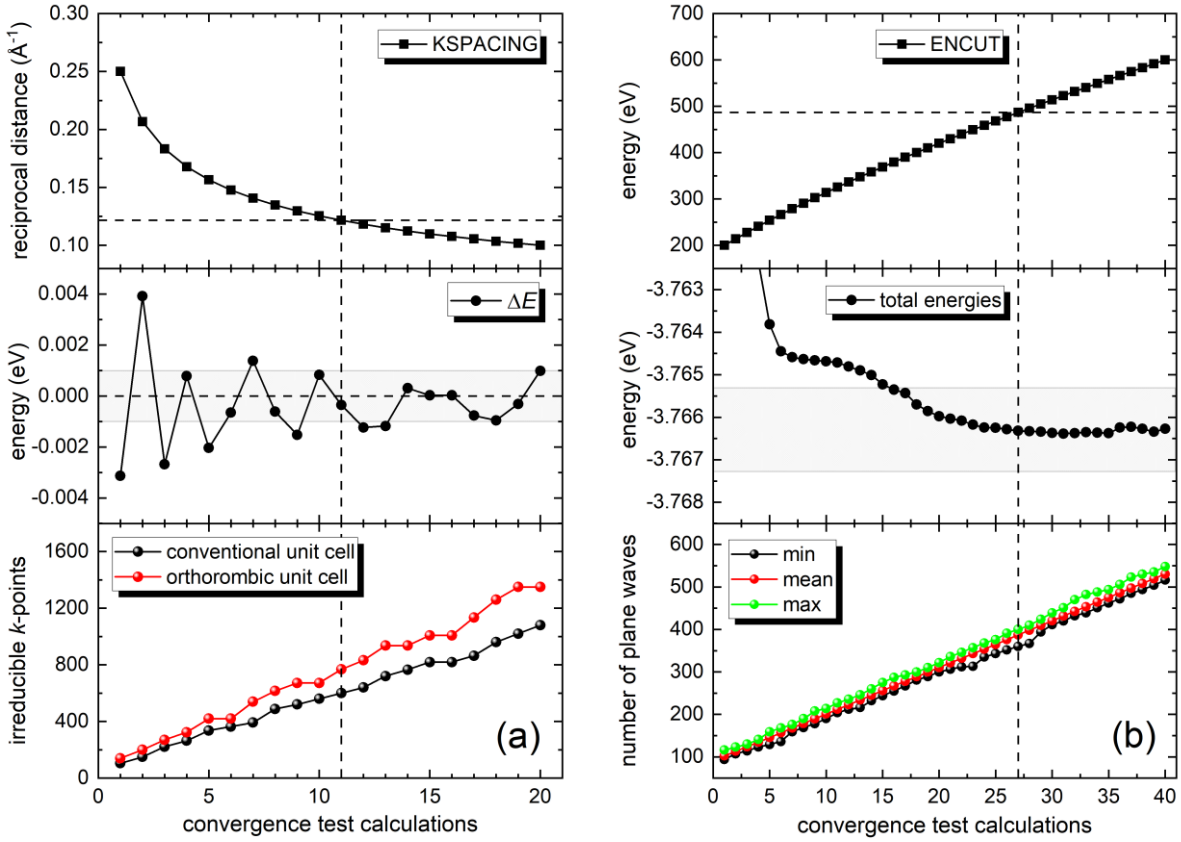

Fig. 1. Summary of KSPACING (a) and ENCUT (b) convergence calculations. Considered values of KSPACING and ENCUT (top panel), total energy differences in different unit cells (middle panel), and resulting numbers of irreducible *k*-points and plane waves (bottom panel).

Moreover, all calculations are carried out with an electronic convergence criterion of EDIFF = 10^{-5} and a force-based ionic convergence criterion of EDIFFG = -0.005 eV/Å. The Fermi step is smeared out using the Methfessel-Paxton scheme of the second order with ISMEAR = 2, where a SIGMA = 0.2 eV is found to result in negligible entropy terms using projector augmented wave pseudopotentials [23] and a generalized gradient approximation for exchange-correlation to Perdew, Burke, and Ernzhof [24]. All *ab-initio* calculations are performed using automatically optimized real space projection operators using LREAL = Auto. Furthermore, all calculations are executed in a spin polarized manner using ISPIN = 2, although most resulted in vanishing magnetic moments as expected. All presented results are based on the crystal structures published in the Materials Project [25]. In particular, structural parameters were established from calculations initiated to Be (mp-87), Ti (mp-46), $Be_{12}Ti$ (mp-1104067), $Be_{17}Ti_2$ (mp-1201649), and Be_2Ti (mp-2749) crystals as reported under the Material IDs in parenthesis.

2.2. Interstitial Hydrogen

Prospective hydrogen interstitial sites were obtained using Voronoi tessellation as implemented in the Python package pymatgen [26]. The procedure is based on the construction of all Voronoi polyhedra for each atom in the considered crystal structure. By definition, each point inside a Voronoi polyhedron (VP) is closer to the central atom, around which the polyhedron is constructed, than to any other atom from this configuration. On this basis, all points on the VP faces are equidistant from two neighboring atoms that have a common face. Points on the VP edges are equidistant from three neighboring atoms, while those on the VP vertices are equidistant from four neighboring atoms. Thus, VP vertices are centers of tetrahedrons and indicate the center of the hole between these atoms. A foreign atom may fit

between matrix atoms whose VPs have a common vertex. Therefore, these positions are suitable for interstitial sites. After structural optimization of the simulation cell performed as described in the previous subsection, candidate interstitial sites are obtained as symmetrically non-equivalent Voronoi nodes obeying additional constraints like minimal distances to each other or to matrix atoms. For each such candidate site, a new structural optimization is set up in an initial structure containing an interstitial hydrogen atom in this candidate site. It is often the case that an atom positioned at a high symmetry position remains there after structural optimization even if the position is an energetic maximum. In order to omit force cancelation due to symmetries, and thus erroneously stabilize some interstitial sites, all symmetries are broken by perturbing every atom in the configuration by a relatively small displacement of 0.01 Å into a random direction. During the optimization of thusly-prepared structures, the hydrogen atom moves from the initial candidate site into an adjacent interstitial site, which is actually stable, if the initial position does not represent a stable minimum. Finally, all these stable interstitial sites are compared to each other as well as their symmetrically equivalent sites according to the symmetry operations of the crystal. Only sites that differ by more than 0.1 Å are then reported as distinct stable interstitial sites for hydrogen in the corresponding subsection of this work.

Note this approach often results in hydrogen relocation from different initial candidate interstitial sites to the same, or symmetrically equivalent, stable interstitial sites. While these cases then contribute only one stable interstitial site, the calculation should not be considered a waste of resources. In fact, every electronically converged iteration contributes valid training data in the sense of new geometrical structures, total energies, and atomic forces. Thus, although the final iterations of such calculations do not contribute new information, the earlier iterations of such energy descents introduce valuable information far away from the energy minima of stable interstitial sites. In this regard, we consider such data particularly valuable, since it samples energies and forces crucial for minimal energy paths of interstitial hydrogen diffusion processes.

2.3. Monovacancies

All non-equivalent monovacancies are identified by means of the SpacegroupAnalyzer class implemented in the pymatgen package [26]. After finding symmetrically equivalent atoms, one representative atom from all these groups is removed, and the resulting monovacancy structure is used as an initial structure for a new VASP calculation. The subsequent structural optimization employing the same parameters as described in subsection 2.1 then results in symmetrically distinct monovacancy structures.

2.4. Monovacancies and interstitial hydrogen

From all Voronoi node-based interstitial site candidates, including symmetrically equivalent ones omitted in the approach described in subsection 2.2, we establish those that are symmetrically equivalent under the reduced symmetry of the relaxed monovacancy structure as obtained after the procedure described in the prior subsection. From these groups of symmetrically equivalent candidate sites, a representative site is selected to add a hydrogen atom into the relaxed monovacancy structure. After a 0.01 Å perturbation of every atom in a random direction to omit force cancelation due to symmetries, a structural optimization with the same parameters described in subsection 2.1 is executed. The resulting stable interstitial sites are then compared to each other, and their symmetrical equivalent sites and all sites differing by more than 0.1 Å are reported in the corresponding subsection of this work.

Note that this approach, similar to that described in subsection 2.2 for interstitial hydrogen, will often result in the shifting of different initial candidate sites to symmetrically equivalent stable sites. Analogously, we consider every single electronically converged

iteration of such calculations valuable information for training sets of future machine learning-based interatomic potentials.

3. Results

3.1. Structure and lattice parameters

It should be noted that according to the phase diagram of the beryllium-titanium [27], there are α-$Be_{17}Ti_2$ (the space group of $P6_3/mmc$) and β-$Be_{17}Ti_2$ (the space group of $R\bar{3}m$). In the present work, only α-$Be_{17}Ti_2$ phase is investigated, since β-$Be_{17}Ti_2$ is unstable at 0 K and transforms into α-$Be_{17}Ti_2$ as indicated in the Materials Project [28]. Therefore, in this paper, α-$Be_{17}Ti_2$ phase is referenced simply as $Be_{17}Ti_2$. In addition, Okamoto [27] has included several new intermediate phases $Be_{10}Ti$, $Be_{13}Ti$, and Be_5Ti_4 in the phase diagram which existence was proposed earlier in Ref. [29] on the basis of measured concentrations of elements. However, to date, there are no reliable experimental data on the crystal structure of these three beryllides. Okamoto also indicated the existence of the phase Be_3Ti with the space group of $R\bar{3}m$. However, according to the data presented in the Materials Project [28], this phase is also unstable and decays into Be_2Ti + Ti.

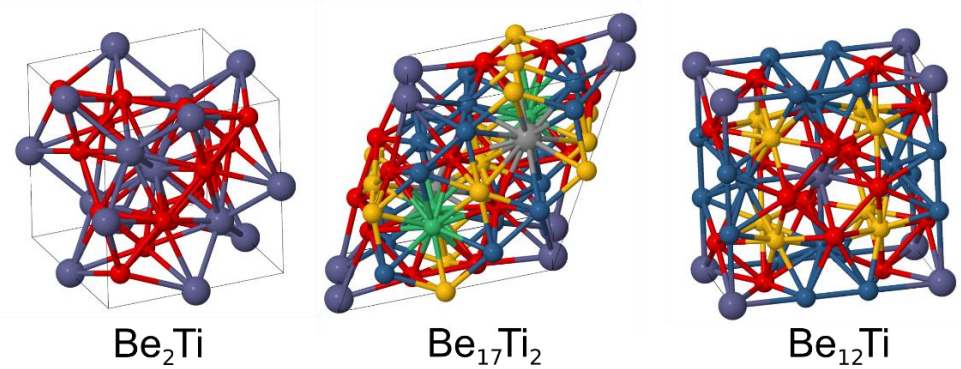

Fig. 2. Crystal structure of the studied titanium beryllides: Be_2Ti (cubic), $Be_{17}Ti_2$ (hexagonal) and $Be_{12}Ti$ (tetragonal). Atoms are colored according to their type: large dark violet and grey spheres represent two crystallographically non-equivalent titanium atoms, while green, yellow, blue and red spheres represent four crystallographic non-equivalent beryllium atoms. The conventional unit cells for beryllides are shown. For a more convenient three-dimensional representation of the crystal lattices, the reader is referred to supplementary materials to this paper.

Table 1. The equilibrium lattice parameters *a* and *c* (Å) at 0 K and zero external pressure, the number of atoms, *N*, and the sizes of the computational cells along three coordinate directions used for *ab initio* calculations of the chosen titanium beryllides.

material	structure	*a*	*c*	cell size	*N*	space group number
Be	hcp	2.267	3.561	3×3×3	54	$P6_3/mmc$ [194]
Ti	hcp	2.923	4.121	3×3×3	54	$P6_3/mmc$ [194]
Be_2Ti	cubic	4.539	–	2×2×2	48	$Fd\bar{3}m$ [227]
$Be_{17}Ti_2$	hexagonal	7.333	7.164	1×1×1	38	$P6_3/mmc$ [194]
$Be_{12}Ti$	tetragonal	7.324	4.151	1×1×2	52	$I4/mmm$ [139]

Crystal lattices of beryllides are rather complex in contrast to, for example, the conventional hcp lattice of beryllium and titanium. The cubic lattice of Be_2Ti with the space group of $Fd\bar{3}m$ contains one beryllium (denoted as Be1[16d]) and one titanium (Ti1[8a]) non-equivalent sites. The corresponding Wyckoff symbols of the atoms are indicated in square brackets. The hexagonal lattice of $Be_{17}Ti_2$ (with the space group of $P6_3/mmc$) contains four beryllium (Be1[4f], Be2[6g], Be3[12j], Be4[12k]) and two titanium (Ti1[2b], Ti2[2d]) non-equivalent sites. The tetragonal lattice of $Be_{12}Ti$ (with the space group of $I4/mmm$) contains four crystallographic non-equivalent sites: three of them are occupied by beryllium (Be1[8f], Be2[8i], Be3[8j]) and one titanium (Ti1[2a]). It is important to note that, for example, atom Be1 in one titanium beryllide phase is not equivalent to atom Be1 in another one, since their Wyckoff symbols (multiplicities) are different. The crystal lattices of the studied titanium beryllides are illustrated in Fig. 2. Owing to the complex crystallography of the beryllides, it is rather challenging to represent their crystal lattices in a comprehensible way in two-dimensional figures. Therefore, we refer the reader to the three-dimensional models of the corresponding crystal lattices included in the supplementary materials to this paper.

For calculations, it is more convenient to use the conventional cell for $Be_{12}Ti$ of the size of 1×1×2 (48 atoms), for $Be_{17}Ti_2$ of the size of 1×1×1 (38 atoms), and the primitive cell for Be_2Ti of the size of 2×2×2 (48 atoms). This is done to ensure that the size of the computational cells and the total number of atoms are more or less comparable with each other for all studied titanium beryllides. The equilibrium lattice constants and angles are: $a = b = c = 4.539$Å and $\alpha = \beta = \gamma = 60°$ for Be_2Ti; $a = b = 7.333$Å, $c = 7.164$Å, $\alpha = \beta = 90°$, and $\gamma = 120°$ for $Be_{17}Ti_2$; $a = b = 7.324$Å, $c = 4.151$Å and $\alpha = \beta = \gamma = 90°$ for $Be_{12}Ti$. It should be noted that the lattice parameters for pure beryllium, pure titanium, and $Be_{12}Ti$ are somewhat different from those obtained in our previous publications [30, 31]. This is mainly due to the use of another set of parameters, namely the plane wave cut-off energy and, in particular, the *k*-point grid.

3.2 Hydrogen in interstitial sites

Hydrogen diffusion in the crystal lattice occurs via an interstitial mechanism, i.e. by jumping from one stable interstitial site into the neighboring one. Therefore, for future calculations of diffusion tensor in the beryllides, which will be published elsewhere, it is important to establish all non-equivalent stable interstitial sites for a hydrogen atom in all of the phases. For quantitative characterization of hydrogen solubility in a material, the solution energy is used, which is defined as

$$E_S^X = E^{X+H} - E^X - \frac{1}{2} \cdot E_{ref}^{H_2}, \quad (1)$$

where E^{X+H} and E^X (here X = Be, Ti, Be_2Ti, $Be_{17}Ti_2$, $Be_{12}Ti$) are the total energies of the computational cell with and without interstitial hydrogen atom, respectively. As a reference point, the energy of one hydrogen atom in a H_2 molecule, i.e. $1/2 \cdot E_{ref}^{H_2} = -3.385$ eV, is used. This choice of the reference energy means that hydrogen solution energy is calculated for the equilibrium established between the given beryllide phase and gas of hydrogen molecules. This situation is typical for the experiments on hydrogen thermal loading of metal.

After energy minimization for all candidate interstitial sites for hydrogen, it turned out that Be_2Ti, $Be_{17}Ti_2$, and $Be_{12}Ti$ phases contain 3, 11 and 7 non-equivalent stable interstitial hydrogen sites, respectively. Pure beryllium and titanium contain only two stable interstitial hydrogen sites, which in the hcp lattice are called basal tetrahedral (conventionally designated as BT) and octahedral (O). In beryllide phases, hydrogen interstitial positions were labeled with letters A, B, … K and sorted according to the increasing solution energy, so that position A has the lowest solution energy and position K has the highest. It should be noted that the stable

interstitial site A in Be_2Ti is not equivalent to the sites A in $Be_{17}Ti_2$ and $Be_{12}Ti$ due to different crystal structures. The same applies to the other interstitial hydrogen sites.

Below, the results for every beryllide are presented and discussed separately, and a comparison with the available literature data, if any, is given. All the results are summarized in Table 2. All non-equivalent stable interstitial hydrogen sites for investigated materials within the used computational cells are illustrated in Fig. 4.

Be_2Ti. The three non-equivalent stable interstitial hydrogen sites within the range of 0.01 to 0.79 eV are revealed. The first one (interstitial site A) is located in the tetrahedron formed by two Be1[16d] atoms and two Ti1[8a] atoms and has the minimum solution energy among the other stable interstitial sites (see Table 2). This indicates that hydrogen can be much easier dissolved in site A in comparison to the other ones with higher solution energy. The second one (interstitial site B) is located in the tetrahedron which is formed by three Be1[16d] atoms and one Ti1[8a] atom, while the third one (interstitial site C) is at the center of the tetrahedron formed by four Be1[16d] atoms and possesses the highest solution energy.

Authors [5] with the use of the first principle calculations as implemented in SIESTA code have found two energetically favorable hydrogen sites in Be_2Ti. As in the present work, the first site is within the tetrahedron formed by two beryllium atoms and two titanium atoms and has the solution energy of −0.52 eV, and the second one is in the tetrahedron formed by one titanium and three beryllium atoms with the solution energy of −0.05 eV. The energy difference between these positions of 0.47 eV is comparable with 0.37 eV between B and A positions in this work. An important difference is that endothermal hydrogen occlusion is suggested here, while the exothermal process is proposed by the negative solution energies calculated in Ref. [5]. The difference in the reference energy of H_2 molecule as well as different *ab initio* codes and pseudopotentials for both metals could be a possible reason for the discrepancy.

Table 2. Non-equivalent stable interstitial sites for hydrogen atoms labeled with letters and sorted in order of increasing solution energy, E_s, calculated with Eq.(1) for the studied titanium beryllides (Be_2Ti, $Be_{17}Ti_2$ and $Be_{12}Ti$) as well as for pure beryllium and titanium metals.

stable interstitial sites	Be	Ti	Be_2Ti	$Be_{17}Ti_2$	$Be_{12}Ti$
A	1.499 (BT)	-0.301 (BT)	0.011	0.127	0.499
B	1.703 (O)	-0.412 (O)	0.380	0.423	0.733
C	–	–	0.792	0.693	0.840
D	–	–	–	0.713	0.895
E	–	–	–	0.787	0.927
F	–	–	–	0.858	0.977
G	–	–	–	0.897	1.271
H	–	–	–	1.042	–
I	–	–	–	1.077	–
J	–	–	–	1.188	–
K	–	–	–	1.235	–

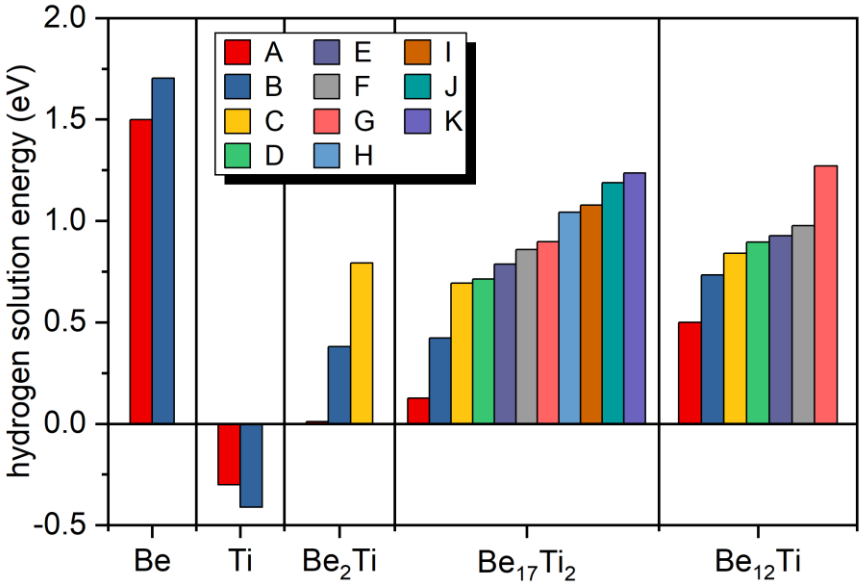

Fig. 3. Solution energy for all non-equivalent stable hydrogen interstitial sites labelled with letters in the studied titanium beryllides (Be_2Ti, $Be_{17}Ti_2$ and $Be_{12}Ti$). Notation of letters A-K is explained in the text. Graphical illustration of the results presented in Table 2.

$Be_{17}Ti_2$. Eleven non-equivalent stable interstitial hydrogen sites within the range of 0.13 to 1.24 eV are found. The interstitial hydrogen (site A) with the minimal solution energy is located in the tetrahedron formed by two Be4[12k] and two Ti1[2b] atoms. The interstitial hydrogen site B is located in the center of a square formed by two Be3[12j] and two Be4[12k] atoms, and one Ti1[2b] and one Ti2[2d] atom, which are at the top and bottom of the plane of this square. The solution energy in site B is about 0.3 eV higher than that for site A (see Table 2). The next five stable hydrogen sites are in the tetrahedrons formed by one titanium and three beryllium atoms. Namely, C (Be3[12j], two Be4[12k], Ti1[2b]), D (two Be3[12j], Be4[12k], Ti1[2b]), E (Be1[4f], Be2[6g], Be4[12k], Ti2[2d]), F (Be2[6g], two Be3[12j], Ti2[2d]), and G (Be2[6g], Be3[12j], Be4[12k], Ti2[2d]). The remaining four interstitial hydrogen sites, with the highest solution energies in comparison to the other sites, are located in the tetrahedra formed by four beryllium atoms, namely the site H (two Be1[4f], two Be3[12j]), I (two Be1[4f], two Be3[12j]), J (Be1[4f], two Be3[12j], Be4[12k]), and K(Be1[4f], Be2[6g], Be3[12j], Be4[12k]). It is interesting to note that the local environment of the two stable sites H and I contains the same types of atoms although positioned at different distances, and their solution energies differ only insignificantly by 0.04 eV. This confirms the fact that the main contribution to hydrogen solution energy is made by the atoms of the nearest environment (atoms forming a tetrahedron), while the influence of atoms located outside this tetrahedron is much less pronounced. Although the initial interstitial hydrogen position was selected near the geometrical center of the respective tetrahedral or octahedral, its final position after relaxation depends on both chemical elements in the direct neighborhood and can be also influenced by the second shell neighbors.

Analysis of the stable interstitial hydrogen sites reveals the following regularities. Namely, the more titanium atoms are in the vertices of a tetrahedron and, accordingly, the fewer beryllium atoms, the lower is hydrogen solution energy at this interstitial site and vice versa. One can conclude that the addition of such exothermal hydrogen occluders, like titanium, promotes hydrogen dissolution.

Kim and co-authors [4] have found ten stable interstitial hydrogen sites in $Be_{17}Ti_2$. Nine out of ten sites have positive values of the solution energy (endothermic) in the range of 0.04

to 1.38 eV, and one site located at the center of the tetrahedron formed by two beryllium and two titanium atoms has negative (exothermic) solution energy of −0.19 eV. As seen in Table 2, no negative values of the solution energy in $Be_{17}Ti_2$ were found in the present study. Unfortunately, it is impossible to unambiguously identify the stable interstitial hydrogen sites revealed in Ref. [4] and compare with those found in this work, since the cited reference does not indicate the specific type of atoms which form tetrahedra or other polyhedra (see Table 1 in [4]). At the same time, the range of the calculated solution energies coincides quite well with that presented in Table 2.

$Be_{12}Ti$. Seven non-equivalent stable interstitial hydrogen sites are consistent with those revealed in our previous publication [31], and the solution energies are within the range of 0.50 to 1.27 eV. However, due to the use of different pseudopotential in the cited work, the values of solution energy for non-equivalent interstitial sites differ by 0.05-0.09 eV from those shown in Table 2 for $Be_{12}Ti$. The lowest hydrogen solution energy is at the octahedral site A surrounded by four Be3[8j] atoms in one plane and two Ti1[2a] atoms located below and above this plane. The highest solution energy is at the site surrounded by two Be1[8f], one Be2[8i] and one Be3[8j] atom. The hydrogen solution energies at sites C (Be1[8f], two Be3[8j], Ti1[2a]) and D (two Be1[8f], Be2[8i], Ti1[2a]) are quite close to each other, suggesting that at a given temperature both sites can be occupied with the same probability. The same applies to the sites E (three Be2[8i], Be3[8j]) and F (four Be2[8i]). The highest hydrogen solution energy of 1.27 eV is at site G surrounded by four beryllium atoms (two Be1[8f], Be2[8i], Be3[8j]) (for details, see Table 2).

Be and *Ti.* Pure beryllium has two non-equivalent stable interstitial hydrogen (basal tetrahedral and octahedral) sites with solution energies of 1.50 and 1.70 eV, respectively. These results are in good agreement with those reported earlier in Refs. [30-32]. As far as energy should be spent to introduce hydrogen inside beryllium, this process is endothermic and hydrogen solubility increases with increasing temperature. The corresponding values of the solution energies for titanium are -0.3 and -0.41 eV (see Table 1), suggesting that hydrogen forms an interstitial solid solution in titanium. Indeed, titanium is known as an exothermic hydrogen occluder, which absorbs hydrogen until at a certain hydrogen concentration a hydride phase starts to form. For such materials, hydrogen solubility decreases with increasing temperature.

Interestingly, in titanium interstitial hydrogen in the basal-tetrahedral site has a higher solution energy than in the octahedral site. As can be clearly seen in Fig. 2 and Table 2, everything is exactly the opposite for beryllium. Such preference for hydrogen ground state might be related to *c*/*a* ratio, which is less than ideal for beryllium and higher than ideal for titanium. In addition, unlike the previous studies [30-32], it turns out that the pseudopotential used in this work leads to the splitting of the basal-tetrahedral sites in both beryllium and titanium. Namely, hydrogen is located not exactly in the plane of the triangle formed by three beryllium atoms (as revealed previously [30]) but has two sites with the minimum energy, which are slightly above and below this plane (see, for example, Fig. 3 from Ref. [30]). Moreover, the distance between these two hydrogen sites in titanium (≈0.8Å) is approximately two times larger than that in beryllium, which is about 0.35Å (see Fig. 4). The latter is associated primarily with a stronger interaction of hydrogen with titanium atoms, and, secondly, to a lesser extent, with the difference in the equilibrium lattice parameter.

A comparison of the results summarized in Table 2 shows that hydrogen solution energy at the basal tetrahedral site (i.e. the most favorable interstitial site in beryllium) is circa 0.71, 0.27 and 0.23 eV higher than the highest solution energy in Be_2Ti, $Be_{17}Ti_2$, and $Be_{12}Ti$, respectively. The latter consistently indicates that occlusion of hydrogen atoms in the studied titanium beryllides occurs easier as compared to pure beryllium.

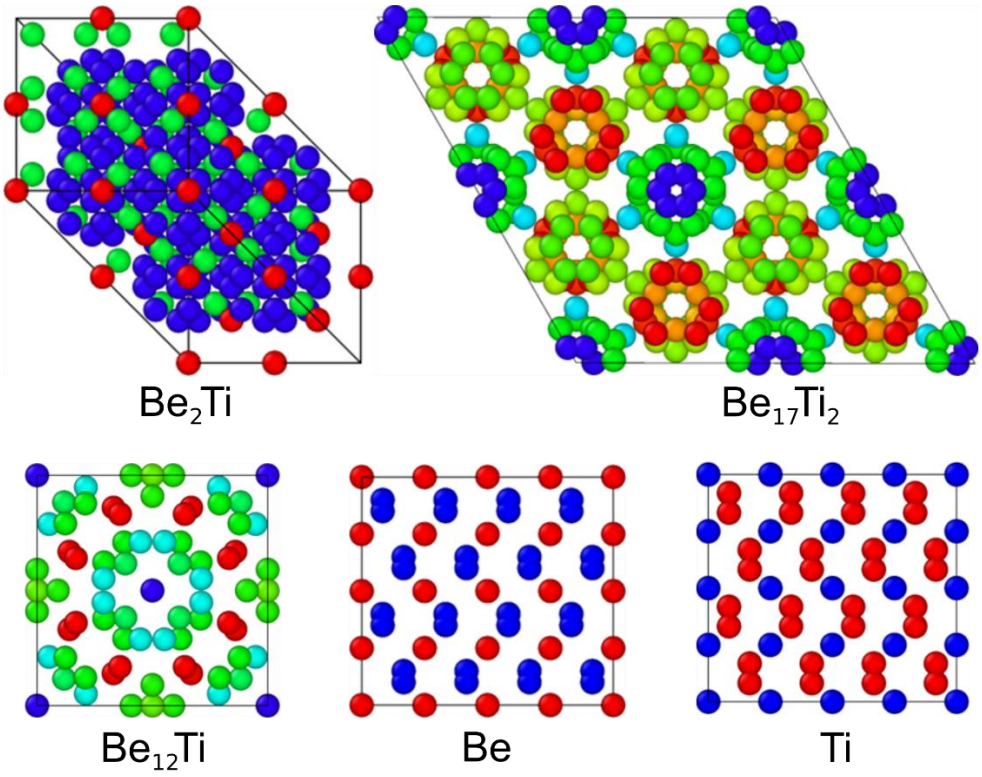

Fig. 4. Non-equivalent stable interstitial hydrogen sites for the studied titanium beryllides (Be_2Ti, $Be_{17}Ti_2$ and $Be_{12}Ti$). Hydrogen atoms are colored according to their binding energy (red corresponds to the maximum binding energy, and blue – to the minimum for each material). For clarity, beryllium and titanium atoms were made invisible and only hydrogen atoms are presented. Perspective depth in all figures was disabled. For a more convenient three-dimensional representation of these hydrogen sites in the corresponding crystal lattices, the reader is referred to supplementary materials in this paper.

3.3 Monovacancy in beryllides

The use of beryllides as neutron multipliers implies operation at high temperatures, as well as intensive fluxes of high-energy neutrons, which cause the generation of substantial amount of point defects, including vacancies. In order to determine which vacancies can be generated in the first place in the considered materials, the formation energies of all non-equivalent vacancy types are calculated via the following formula:

$$E_f^X = E^{X+V} - E^X + E_{coh}^{Be,Ti}, \quad (2)$$

where E^{X+V} is the total energy of the computational cell with a monovacancy V (here V = Be1, Be2, Be3, Be4, Ti1, Ti2), and E^X is the total energy of the perfect cell; E_{coh}^{Be} = -3.766 eV and E_{coh}^{Ti} = -7.763 eV are the cohesive energies of hcp beryllium and titanium lattices, respectively. As follows from expression (2), bulk hcp beryllium and titanium are chosen as the reference solids. The vacancy formation energies for the titanium beryllides are presented in Fig. 5 and summarized in Table 3. It is important to note that Be*i*/Ti*i* vacancy in one beryllide is not crystallographically equivalent to that in another one due to different crystal structure of the beryllides, and therefore a direct comparison between them by looking at the same sublattice index might be misleading.

For $Be_{17}Ti_2$ and $Be_{12}Ti$, the formation energy of beryllium vacancies is circa two times smaller than the corresponding energy for titanium vacancies. This seems to be reasonable,

since the atomic radius of titanium is about 30% larger than that of beryllium. Therefore, it can be expected that at elevated temperatures in stoichiometric compounds beryllium vacancies will be available in a higher concentration in contrast to titanium vacancies. In addition, the minimum and maximum values of the formation energy of beryllium vacancies differ slightly from each other, i.e., by 0.25 eV for $Be_{17}Ti_2$ and 0.21 eV for $Be_{12}Ti$, suggesting that in both beryllides at high temperatures all beryllium vacancies regardless of their sublattice type can be generated. The exception is Be_2Ti, in which the formation energies of Be1 and Ti1 vacancies does not differ much from each other, namely 2.22 vs. 2.60 eV. This can be rationalized from the fact that the crystal lattice of Be_2Ti is less dense in contrast to the lattices of the other studied beryllides. The volume per atom in Be_2Ti is 10.92 $Å^3$, while 8.77 $Å^3$ for $Be_{17}Ti_2$ and 8.56 $Å^3$ for $Be_{12}Ti$. Presently, we are aware of the two publications [33, 34] in which the vacancy formation energies were calculated only in $Be_{12}Ti$ (shown in Table 3 for comparison). The results obtained in the this study are in good agreement with the previous calculations [33, 34], especially taking into account the fact that in these papers different computer codes [34] and different pseudopotentials [33] were used.

Table 3. Vacancy formation energies (in eV) for the studied titanium beryllides (Be_2Ti, $Be_{17}Ti_2$ and $Be_{12}Ti$) calculated for all non-equivalent vacancy positions at 0 K and zero external pressure. A dash in a column means that this type of vacancy does not exist in a particular metal or beryllide. For comparison, the lower part of the table also shows the available results on the vacancy formation energy taken from the literature.

material	Be1	Be2	Be3	Be4	Ti1	Ti2
Be	0.86	–	–	–	–	–
Ti	–	–	–	–	2.02	–
Be_2Ti	2.22	–	–	–	2.60	–
$Be_{17}Ti_2$	1.83	1.95	2.08	1.91	4.08	4.19
$Be_{12}Ti$	1.79	1.58	1.65	–	4.23	–
$Be_{12}Ti$ [33]	1.65	1.44	1.56	–	3.92	–
$Be_{12}Ti$ [34]	1.60	1.43	1.53	–	4.10	–
$Be_{12}Ti$ [35]	1.66	1.45	1.57	–	3.95	–

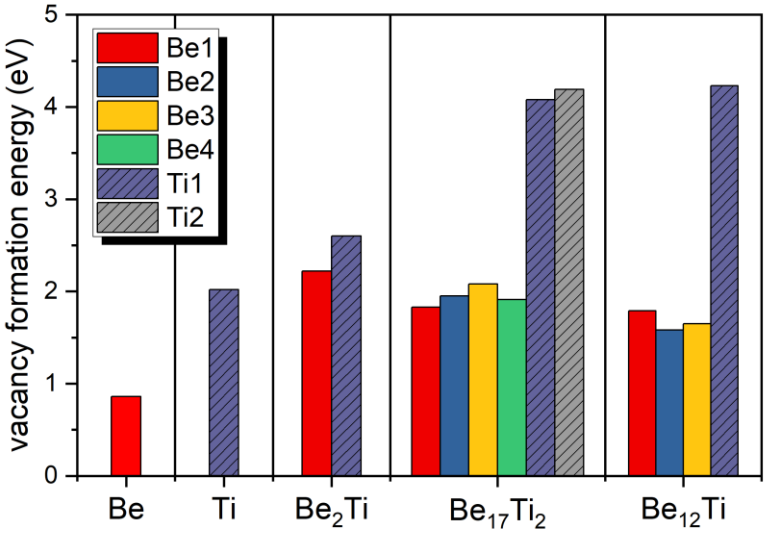

Fig. 5. Vacancy formation energies calculated for various titanium beryllides (Be_2Ti, $Be_{17}Ti_2$ and $Be_{12}Ti$) and for pure metals (Be, Ti). Bars are colored according to the sublattice where vacancy was created.

3.4 Trapping of hydrogen in beryllides monovacancies

Vacancies and their clusters in beryllium are known to be efficient traps for hydrogen atoms. A deeper understanding of hydrogen trapping is an important issue in terms of reduction of radioactive waste for future fusion reactors. Thus, binding of hydrogen with traps controls its release out of material, in particular, during thermal desorption experiments. Below binding of a single hydrogen atom with beryllium and titanium monovacancies is considered. In this case, in contrast to previous works [30, 36], hydrogen is considered to be located not only directly inside a vacancy, but also in all non-equivalent interstitial positions in the vicinity of the vacancy within the computational cell. This is done from the considerations that, generally speaking, hydrogen might be attracted by a vacancy being at some distance from it. This reasoning is based on the studies in which the binding energy of an impurity atom with a vacancy in iron was calculated. In particular, by means of *ab initio* calculations it was found that nickel atom at the distance of the second nearest neighbor has even higher binding energy with iron vacancy than at the distance of the first nearest neighbor [37]. Alternatively, another example, the binding energy of the copper atom at the distance of the third and fourth nearest neighbors is practically absent, while at a distance of the fifth nearest neighbor it appears again [37].

A quantitative characteristic, allowing to estimate how strongly hydrogen atom is bound with a monovacancy *V* (where *V* = Be1, Be2, Be3, Be4, Ti1, Ti2), is the binding energy, which can be calculated according to the following expression:

$$E_b^X = E^{X+V+H} - E^{X+V} + E^{X+H} - E^X, \quad (3)$$

where E^{X+V+H} is the total energy of the configuration with a monovacancy *V* and one hydrogen atom; E^{X+V} is the total energy of the computational cell containing a monovacancy *V*; E^{X+H} is the lowest energy configuration containing one hydrogen atom at an interstitial site in material *X* (here *X* = Be, Ti, Be_2Ti, $Be_{17}Ti_2$, $Be_{12}Ti$), which is used as a reference point; E^X is the total energy of the perfect lattice in material *X*. This sign convention implies that positive values of binding energy mean attraction, while negative values – repulsion between monovacancy and a hydrogen atom.

Fig. 6 summarizes all the results obtained for three titanium beryllides (Be_2Ti, $Be_{17}Ti_2$, $Be_{12}Ti$) as well as for beryllium and titanium. The binding energies of a hydrogen atom, which is considered to be located in all non-equivalent sites within the computational cell containing a monovacancy vs. sequential configuration index are presented. Note that, in this particular case, the binding energies of the structures are sorted in descending order along the abscissa axis, and the index of the configuration does not have any physical meaning. Since the studied materials contain a different number of non-equivalent hydrogen sites, for ease of comparison, the normalized index is used along the abscissa axis. The higher binding energy is an indicator of the fact that hydrogen is in a monovacancy, while binding energy tends to reduce with the distance from a monovacancy in all studied beryllides.

In the subsections below, the results for every beryllide are presented and discussed separately, and a comparison with the available data in the literature, if any, is given. All non-equivalent vacancies and their next-nearest shell atomic environment in the titanium beryllides are illustrated in Fig. 7. Vacancies are marked for clarity with a transparent sphere centered at the removed atom. To maintain clarity and not overload the figure, only interstitial hydrogen sites with positive binding energies are shown, i.e., those in which hydrogen is bounded to the vacancy. Hydrogen atoms are colored according to their binding energy with the vacancy calculated according to Eq. (3).

3.4.1 *Be and Ti*

Pure hcp beryllium and titanium metals contain only one type of crystallographically non-equivalent vacancies: Be1 and Ti1. The number after the vacancy type (which is beryllium or titanium) corresponds to that introduced in paragraph 3.1. It should be noted that despite having the same hcp crystal lattice type for both beryllium and titanium, the stable hydrogen sites both inside and outside the vacancy are different for these metals.

Be1 vacancy. Inside the vacancy, the stable hydrogen sites form a trigonal bipyramid with base and side edge lengths of approximately 1.84Å and 1.44 eV, respectively. The binding energy of hydrogen atoms at the vertices and at the triangular base are 1.0 eV and 1.13 eV, correspondingly. Outside the vacancy, at two hydrogen sites next to each other which are above the Be-Be bond, the binding energy is 0.26 eV, and over the beryllium atom, the binding energy is 0.04 eV. The hydrogen binding energy is rather low (~0.1 eV) at positions below and above the triangle formed by beryllium atoms.

Ti1 vacancy. Inside the vacancy, at the base of the triangular bipyramid (double sites very close to each other), the binding energy is 0.24 eV. At the vertices of the triangular bipyramid, the binding energy of hydrogen atoms with the vacancy is negligible and equal to 0.05 eV. Hydrogen atoms located on the inner wall of the vacancy, namely at the center of the square formed by four titanium atoms, have a binding energy of 0.23 eV. Outside the vacancy, above the triangle formed from titanium atoms, the binding energy is rather insignificant and in the range of 0.04 to 0.08 eV.

Thus, even though beryllium and titanium have the same crystal structure, the stable hydrogen sites inside and outside the vacancy are slightly different. In both cases, the stable hydrogen sites form a triangular bipyramid inside the vacancy. Inside the titanium vacancy, there are more stable hydrogen sites, while in the beryllium vacancy, there are more hydrogen sites with a positive binding energy outside the vacancy.

3.4.2 Be_2Ti.

There are only two non-equivalent monovacancy types for this beryllide, namely one Be1 and one Ti1.

Be1 vacancy. Hydrogen atoms inside the vacancy have a binding energy of 0.46 eV and are located above the triangle formed by one titanium and two beryllium atoms. Note that hydrogen does not have a stable position in the triangle formed by three beryllium atoms. The latter means that hydrogen prefers to be situated near a titanium atom, where the electron density is higher than that in the vicinity of a beryllium atom [38]. Inside the vacancy, there are hydrogen sites with a relatively low positive binding energy of 0.1 eV, namely in the triangle formed by one titanium and two beryllium atoms.

Ti1 vacancy. Inside the vacancy, there are two stable non-equivalent hydrogen sites. The first site is above the Be1-Be1 bond, where hydrogen has a binding energy of 0.36 eV, while the second site is above the triangle formed by three beryllium atoms with a slightly lower binding energy of 0.25 eV. Outside the vacancy, there exist two non-equivalent hydrogen sites with positive binding energy. Hydrogen disposed above the quadrangle formed by two beryllium and two titanium atoms has a binding energy of 0.12 eV. In the second site, which is above the Be1-Ti1 bond, the binding energy is rather small and equal to 0.03 eV. The latter means that liquid nitrogen temperature hydrogen in this site will not be bound to the vacancy. It can easily jump out of this site, overcoming such low binding energy.

3.4.3 $Be_{17}Ti_2$.

This beryllide contains six non-equivalent monovacancy types: four beryllium vacancies (Be1, Be2, Be3, Be4) and two titanium vacancies (Ti1 and Ti2).

Be1 vacancy. Inside the vacancy, there are three non-equivalent hydrogen sites with binding energies of 0.41, 0.34, and 0.27 eV. In the first and the second cases, the hydrogen is located above the triangle formed by one titanium and two beryllium atoms. A small difference in energy, i.e., 0.41 vs. 0.34 eV, is related to the different distances from the center of the vacancy. In the third case, hydrogen is exactly in the middle between two titanium atoms. The binding energy of hydrogen atoms located outside the vacancy is quite small and in the range of 0.02-0.13 eV.

Be2 vacancy. Interstitial hydrogen with the highest binding energy of 0.56 eV is located between two titanium atoms. However, hydrogen is not situated exactly on the line connecting two titanium atoms but is somewhat deviated from it. This is due to the proximity of two beryllium atoms. Another hydrogen site inside the vacancy with a high binding energy of 0.44 eV is above the triangle formed by one titanium and two beryllium atoms. The remaining hydrogen atoms inside the vacancy have binding energy in the range of 0.16-0.21 eV and are near the titanium atom. Hydrogen in the sites located outside the vacancy has a binding energy of 0.16 eV and is above the Be-Ti bond.

Be3 vacancy. Hydrogen atoms inside the vacancy have a binding energy of 0.36 eV and are located above the triangle formed by one titanium and two beryllium atoms and slightly offset from the line connecting two titanium atoms. In the outer two sites, hydrogen is weakly bonded to the vacancy with the energy of 0.07 eV and is in the middle of the bond between two beryllium atoms. Note that in this case, there are no hydrogen sites with a positive binding energy near the titanium atom.

Be4 vacancy. Hydrogen in interstitial sites inside the vacancy has binding energies of 0.34 and 0.25 eV. These sites form a ring and are located near the titanium atom. The atoms outside the vacancy possess the lower binding energies of 0.16 and 0.04 eV. In the first case, the atoms form a regular hexagon and are located between titanium atoms approximately on the same level as the hydrogen atoms inside the vacancy. In the second case, hydrogen atoms are also located between titanium atoms (the upper titanium atom is not shown because it goes beyond the computational cell), but with a slightly lower binding energy. This is because the latter group is more distant from the vacancy, in contrast to those with higher binding energy located below.

Ti1 vacancy. There is a fairly large number of hydrogen sites with positive binding energy. Six sites located near the titanium atom have a binding energy of 0.21 eV. Other hydrogen atoms inside the vacancy have a rather low binding energy of 0.02 eV and are located above the triangle formed by three beryllium atoms. Hydrogen atoms that are outside the vacancy having a positive binding energy with it were not found.

Ti2 vacancy. This is the only case among all the cases studied for which no hydrogen sites with a positive binding energy inside the vacancy were detected. Hydrogen atoms outside the vacancy form a regular hexagon. They all have the same binding energy of 0.16 eV and are located in the middle between two titanium atoms.

3.4.4 $Be_{12}Ti$.

According to the symmetry of the lattice, there exist three non-equivalent monovacancies on beryllium sites (Be1, Be2, Be3) and one vacancy on titanium sites (Ti1).

Be1 vacancy. There are two hydrogen sites (which are symmetrically equivalent to each other) inside the vacancy with a high binding energy of 0.75 eV. These sites are not located above the titanium atom and are not equidistant from other beryllium atoms, but are displaced towards two beryllium atoms and thus are located above the triangle formed by one titanium and two beryllium atoms. Hydrogen atoms located outside the vacancy have a rather low binding energy

of 0.08 eV. Both of these outer atoms are located above the triangle formed from one titanium and two beryllium atoms.

Be2 vacancy. Six equivalent hydrogen sites located in the vicinity of titanium atoms and inside the hexagon formed by beryllium atoms have the same binding energy of 0.63eV. The other three hydrogen atoms inside the vacancy are located above three beryllium atoms and have a binding energy of 0.21 eV. The outer interstitial hydrogen atoms, which are between two titanium and two beryllium atoms, are weakly bounded with the vacancy (0.04 eV).

Be3 vacancy. Inside the vacancy, hydrogen located in the center of a quadrangle formed by two titanium and two beryllium atoms has a binding energy of 0.50 eV. A hydrogen atom is most strongly bound to this vacancy and has the highest binding energy of 0.60 eV when it is above the triangle formed by one titanium and two beryllium atoms. The binding energies of hydrogen atoms located on the edges of the hexagon are in the range of 0.42-0.45 eV. There are no hydrogen positions with positive binding energy outside this vacancy. Depending on local atomic environment, hydrogen located on the bond between two beryllium atoms has two different binding energies of 0.15 and 0.21 eV.

Ti1 vacancy. The binding energy of hydrogen, which is located inside the vacancy and in the center of a quadrangle formed by beryllium atoms, is 0.34 eV. The other inner hydrogen atoms have binding energies in the range of 0.14-0.34 eV. The outer hydrogen atoms located above the triangle formed by three beryllium atoms are symmetrically equivalent. They are bounded by the vacancy and have the same binding energy of 0.12 eV.

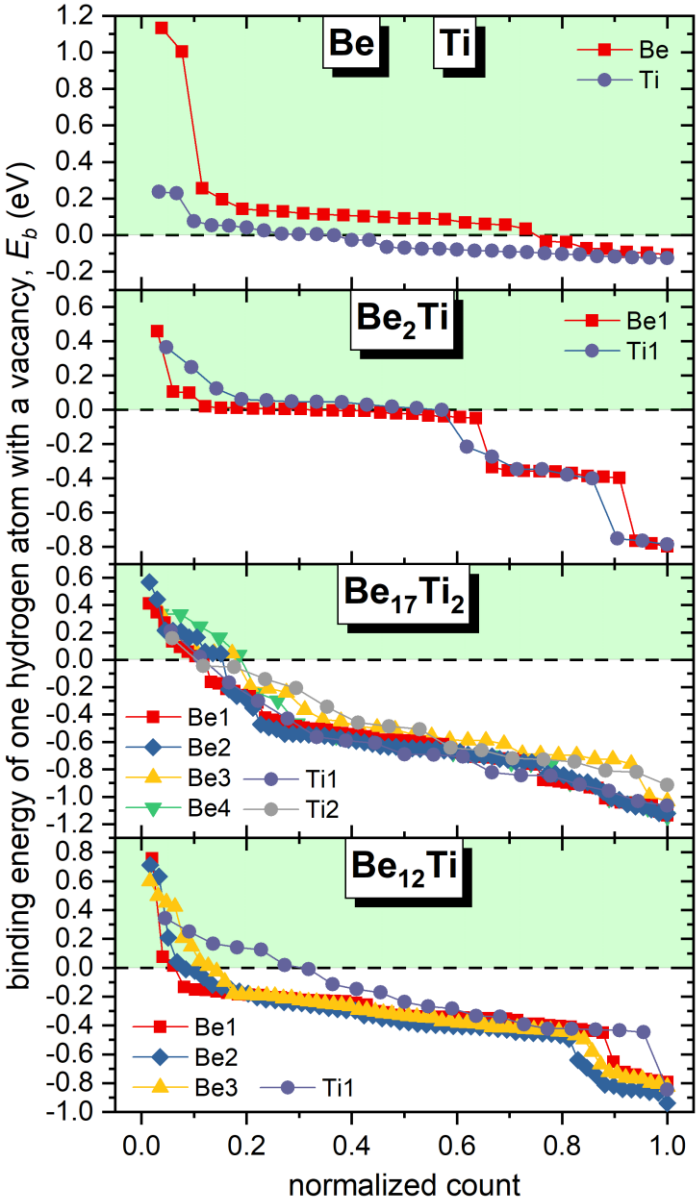

Fig. 6. Binding energy of one hydrogen atom located in all non-equivalent sites within different types of monovacancies in various titanium beryllides (Be_2Ti, $Be_{17}Ti_2$ and $Be_{12}Ti$). Hydrogen is positioned not only inside a monovacancy, but also in all non-equivalent interstitial positions outside a monovacancy within the computational cell. Non-equivalent nodes are arranged in decreasing order of the binding energy. For each material, the region of positive binding energies is highlighted in light green, that is, where the hydrogen atom is bonded to a vacancy.

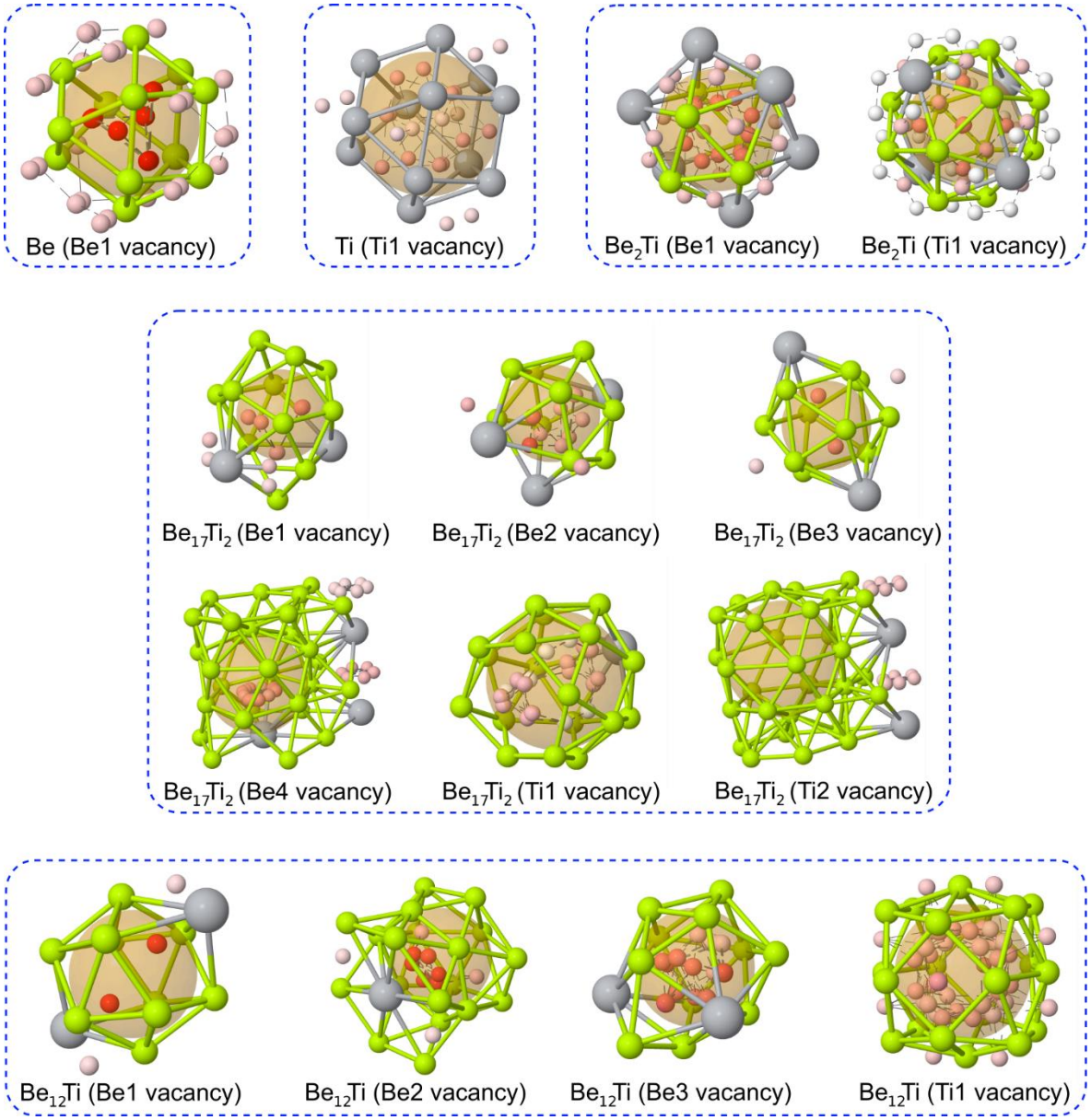

Fig. 7. The next-nearest shell atomic environment for all non-equivalent types of monovacancies in the studied titanium beryllides (Be_2Ti, $Be_{17}Ti_2$ and $Be_{12}Ti$) and hcp beryllium and titanium. For clarity, the vacancy is represented as a transparent sphere centered on the removed atom. Hydrogen atoms are colored according to their binding energy calculated using the expression (3). Only hydrogen sites with positive binding energy, implying attraction between vacancy and hydrogen, are displayed. The other hydrogen sites with negative binding energy both inside and outside the vacancies are made invisible. Beryllium atoms are colored in light green (without reference to their non-equivalence in the crystal lattice), and titanium atoms with a larger radius are shown in gray.

4. Discussion

Our calculations consistently yield a total magnetization of 1.1 μ_B per unit cell of Be_2Ti, which is in good agreement with results obtained within the Materials Project [25], cf. ID mp-2749. Within the Be_2Ti structure, titanium ions are associated with parallel contributions of about $1.1\mu_B$, while beryllium ions provide no significant contributions to the total magnetization. Although our calculations generally consider fewer electrons per unit cell by deploying correspondingly different pseudopotentials and differ in many important VASP parameters, starting from the results obtained within the Materials Project [25] as described at the end of section 2.1 entails the same approach to choosing initial magnetic moments. As this consists of rather large parallel magnetic moments at the very beginning of the first electronic minimizations, erroneous magnetizations as an artifact of initially parallel magnetic moments were precluded. To that end, additional calculations deploying antiparallel moments for titanium ions were carried out, all of which consistently reproduce the same total magnetization of about $1.1\mu_B$ from parallel contributions at titanium ions.

Recently Zhu et al. [36] have performed first-principle calculations of the trapping energies for hydrogen-vacancy complexes in $Be_{12}Ti$. The trapping energy was calculated using an expression similar to formula (3) used in this work for binding energy, and stable configurations of hydrogen atom inside four crystallographically non-equivalent monovacancies were reported. Note that the authors [36] also calculated the contribution of zero-point energy to the binding energy of hydrogen with vacancies and found that the energy trend remains unchanged. However, as it turned out, this contribution for one hydrogen atom inside vacancy is rather insignificant, except for vacancy Be2 in the notation adopted in this article (see Fig. 3 in Ref. [36]). Further, the binding energies will be compared only without taking into account the zero-point energy correction. Authors [36] established that hydrogen atom is trapped in Be1 vacancy (Be6 in our notation) and the most stable configuration (above the triangle formed by one titanium and two beryllium atoms) has the binding energies of 0.763 eV, which is very close to that found above. Hereinafter, for a complete understanding of the arrangement of atoms within the vacancies, we refer the reader to the figures given in the original publication [36]. For Be2 vacancy (Be12 in our notation), the hydrogen stable site is at the center of a hexagon formed by six beryllium atoms and exactly above the titanium atom and has a binding energy of 0.66 eV. This result is slightly different from that presented in the present study. Namely, inside the indicated hexagon of beryllium atoms, there are six equivalent positions for a hydrogen atom with a very similar binding energy of 0.63 eV. The results obtained for the Be3 vacancy (Be22 in our notation) are partially consistent with our results. According to Fig. 4 in Ref. [36], in the stable configuration, hydrogen atom is located between two titanium atoms and has a binding energy of 0.505 eV. Indeed, this hydrogen site is found to be stable, however, it is not characterized by the highest binding energy. As shown above, hydrogen located above the triangle formed by one titanium and two beryllium atoms has the highest binding energy of 0.60 eV (see Fig. 6). The most stable configuration of a hydrogen atom in titanium vacancy (Ti0 in our notation) is at the center of a quadrangle formed by beryllium atoms and with a binding energy of 0.338 eV, which almost exactly coincides with that obtained in this work, i.e. 0.34 eV.

The calculations performed in this work can be compared with the experimental results obtained by Chakin et al. [39]. In particular, the authors performed thermal-programmed desorption and evaluated tritium retention in titanium beryllide Be-7at.%Ti and pure beryllium after neutron irradiation up to damage doses. Note that Be-7Ti contained two main phases: the main $Be_{12}Ti$ and a small amount of beryllium so its initial chemical composition was 71.2 wt.% beryllium and 28.5 wt.% titanium. It turned out that tritium retention from Be-7Ti is essentially lower (at higher temperatures by more than 10 times) than that in beryllium. The latter means that hydrogen is more weakly bound to the traps, i.e., has a lower binding energy, which is

thoroughly confirmed by the corresponding calculations presented in Fig. 6. It should also be noted that a more accurate quantitative comparison cannot be made, since the evaluation of tritium retention was carried out at high temperatures of 710-1040 K, while *ab initio* calculations at absolute zero temperature. Nevertheless, there is every reason to believe that such a ratio between the binding energies of hydrogen in titanium beryllides and pure beryllium will be preserved with increasing temperature, which certainly requires a separate study.

5. Conclusions

Hydrogen behavior in three titanium beryllides (Be_2Ti, $Be_{17}Ti_2$, $Be_{12}Ti$) as well as in pure beryllium and titanium were investigated with the use of *ab initio* methods. Hydrogen solution energies at interstitial sites as well as binding energies with monovacancies were calculated. The main conclusions are the following.

Hydrogen dissolution in the titanium beryllides should occur easier than in pure beryllium. The solution energies in all the beryllides are approximately the same order indicating that hydrogen should be approximately uniformly dissolved in the structure containing inclusions of these three phases.

The formation energy of Be vacancies in $Be_{17}Ti_2$ and $Be_{12}Ti$ is circa two times less than that for titanium vacancies, while they are almost equal in Be_2Ti. The latter means that the formation of titanium vacancies in $Be_{17}Ti_2$ and $Be_{12}Ti$ is less likely, in contrast to beryllium vacancies. At the same time, in Be_2Ti, such vacancies should form with approximately the same probability, but with a slight predominance of beryllium vacancies. The formation energy of beryllium vacancies in all studied beryllides is at least two times higher than that in pure beryllium. The same applies to titanium vacancies.

Some hydrogen atoms located outside the vacancies can be bonded with vacancies with binding energy up to 0.30 eV. Hydrogen inside a monovacancy, as a rule, has a higher binding energy as compared to hydrogen atoms outside this vacancy. Interstitial hydrogen is slightly attracted by vacancies even in their vicinity. At low temperatures, this provides additional trapping sites outside of vacancies. The hydrogen binding energy with the vacancies in titanium beryllides is lower than that in pure beryllium. This indicates that hydrogen is more weakly trapped in beryllides and released from them at lower temperatures than from beryllium.

Acknowledgments

This work has been carried out within the framework of the EUROfusion Consortium, funded by the European Union via the Euratom Research and Training Programme (Grant Agreement No 101052200 — EUROfusion). Views and opinions expressed are however those of the author(s) only and do not necessarily reflect those of the European Union or the European Commission. Neither the European Union nor the European Commission can be held responsible for them. High-performance computing resources were provided by the EUROfusion within Joint EU-JA HPC Simulation Project BERYLLID and 4th Cycle Project BeFusion and performed at the High-Performance Computers Marconi-Fusion (Bologna, Italy) and Japan Fusion Reactor Simulator (JFRS-1) at Computational Simulation Centre of the International Fusion Energy Research Centre, Rokkasho, Japan.

References

[1] P. Vladimirov, D. Bachurin, V. Borodin, V. Chakin, M. Ganchenkova, A. Fedorov, M. Klimenkov, I. Kupriyanov, A. Moeslang, M. Nakamichi, T. Shibayama, S. Van Til, M. Zmitko, Current Status of Beryllium Materials for Fusion Blanket Applications, Fusion Sci Technol 66(1) (2014) 28-37.
[2] P.V. Vladimirov, V.P. Chakin, M. Durrschnabel, R. Gaisin, A. Goraieb, F.A.H. Gonzalez, M. Klimenkov, M. Rieth, R. Rolli, N. Zimber, S. Udartsev, M. Kolmakov, A. Vechkutov, E. Frants, Development and characterization of advanced neutron multiplier materials, J Nucl Mater 543 (2021) 152593.
[3] Y. Fujii, M. Miyamoto, J.-H. Kim, M. Nakamichi, N. Murayoshi, H. Iwakiri, Hydrogen retention behavior of beryllides as advanced neutron multipliers, Nucl Mater Energy 9 (2016) 233-236.
[4] J.H. Kim, H. Iwakiri, T. Furugen, M. Nakamichi, Synthesis and reactivity of single-phase Be17Ti2 intermetallic compounds, Fusion Eng Des 102 (2016) 44-49.
[5] J.H. Kim, H. Iwakiri, M. Nakamichi, Reactivity with water vapor and hydrogen storage capacity of Be2Ti compound, International Journal of Hydrogen Energy 41(21) (2016) 8893-8899.
[6] J.H. Kim, M. Nakamichi, The effect of sintering time on synthesis of plasma sintered beryllides, J Nucl Mater 442(1-3) (2013) S461-S464.
[7] M. Nakamichi, J.H. Kim, K. Yonehara, Novel granulation process of beryllide as advanced neutron multipliers, Fusion Eng Des 88(6-8) (2013) 611-615.
[8] J.H. Kim, M. Nakamichi, Preliminary synthesis and mechanical property of titanium beryllide pebbles with different chemical compositions, J Alloy Compd 585 (2014) 63-68.
[9] J.H. Kim, M. Nakamichi, Synthesis and characteristics of ternary Be-Ti-V beryllide pebbles as advanced neutron multipliers, Fusion Eng Des 109 (2016) 1764-1768.
[10] M. Nakamichi, J.H. Kim, K. Ochiai, Beryllide pebble fabrication of Be-Zr compositions as advanced neutron multipliers, Fusion Eng Des 109 (2016) 1719-1723.
[11] J.H. Kim, M. Nakamichi, Fabrication and characterization of Be-Zr-Ti ternary beryllide pebbles, Fusion Eng Des 136 (2018) 864-868.
[12] M. Nakamichi, J.H. Kim, Prevention of hydrogen generation reaction with water vapor by surface modification of beryllides as advanced neutron multipliers, Fusion Eng Des 124 (2017) 905-909.
[13] M. Zmitko, P. Vladimirov, R. Knitter, M. Kolb, O. Leys, J. Heuser, H.C. Schneider, R. Rolli, V. Chakin, S. Pupeschi, L. Magielsen, A. Fedorov, Y. Poitevin, Development and qualification of functional materials for the European HCPB TBM, Fusion Eng Des 136 (2018) 1376-1385.
[14] F.A. Hernandez, P. Pereslavtsev, G.M. Zhou, B. Kiss, Q.L. Kang, H. Neuberger, V. Chakin, R. Gaisin, P. Vladimirov, L.V. Boccaccini, G.A. Spagnuolo, S. D'Amico, I. Moscato, Advancements in the Helium-Cooled Pebble Bed Breeding Blanket for the EU DEMO: Holistic Design Approach and Lessons Learned, Fusion Sci Technol 75(5) (2019) 352-364.
[15] R. Gaisin, V. Chakin, P. Vladimirov, F.A. Hernandez, S. Udartsev, A. Vechkutov, M. Kolmakov, Industrial-scale manufacturing experience of titanium beryllide block for DEMO blanket application, Fusion Eng Des 161 (2020) 111862.
[16] R. Gaisin, V. Chakin, M. Duerrschnabel, R. Rolli, T. Weingaertner, A. Goraieb, P. Vladimirov, Effect of HIP at 800 and 900 degrees C on microstructure and properties of extruded Be-Ti composites, Nucl Mater Energy 24 (2020) 100771.
[17] R. Gaisin, V. Kuksenko, M. Duerrschnabel, V. Chakin, A. Goraieb, P. Vladimirov, Effect of HIP at 1000-1200 degrees C on microstructure and properties of extruded Be-Ti composites, Nucl Mater Energy 30 (2022) 101128.

[18] J.H. Kim, M. Nakamichi, Comparative study on arc-melted and plasma-sintered beryllides, J Alloy Compd 546 (2013) 171-175.
[19] R. Gaisin, V. Chakin, R. Rolli, J. Hoffmann, H. Leiste, T. Bergfeldt, U. Jantsch, M. Klimenkov, J. Lorenz, A. Goraieb, P. Vladimirov, A. Moslang, Synthesis of Be12Ti compound via arc melting or hot isostatic pressing, J Alloy Compd 818 (2020) 152919.
[20] https://vasp.at/vasp-workshop/accuracy.pdf, P. 29.
[21] https://www.vasp.at/wiki/index.php/KSPACING.
[22] https://www.vasp.at/wiki/index.php/ENCUT.
[23] G. Kresse, D. Joubert, From ultrasoft pseudopotentials to the projector augmented-wave method, Phys Rev B 59(3) (1999) 1758-1775.
[24] J.P. Perdew, K. Burke, M. Ernzerhof, Generalized gradient approximation made simple, Phys Rev Lett 77(18) (1996) 3865-3868.
[25] A. Jain, S.P. Ong, G. Hautier, W. Chen, W.D. Richards, S. Dacek, S. Cholia, D. Gunter, D. Skinner, G. Ceder, K.A. Persson, Commentary: The Materials Project: A materials genome approach to accelerating materials innovation, Apl Mater 1(1) (2013) 011002.
[26] S.P. Ong, W.D. Richards, A. Jain, G. Hautier, M. Kocher, S. Cholia, D. Gunter, V.L. Chevrier, K.A. Persson, G. Ceder, Python Materials Genomics (pymatgen): A robust, open-source python library for materials analysis, Comp Mater Sci 68 (2013) 314-319.
[27] H. Okamoto, Be-Ti (beryllium-titanium), J Phase Equilib Diff 29(2) (2008) 202-202.
[28] The Materials Project: https://materialsproject.org/.
[29] I. Ohnuma, R. Kainuma, M. Uda, T. Iwadachi, M. Uchida, H. Kawamura, K. Ishida, Phase Equilibria in the Be-V and Be-Ti Binary Systems, 6th IEA international workshop on beryllium technology for fusion, Japan Atomic Energy Research Institute, Japan, 2004, pp. 172-183.
[30] D.V. Bachurin, P.V. Vladimirov, Ab initio study of Be and Be12Ti for fusion applications, Intermetallics 100 (2018) 163-170.
[31] D.V. Bachurin, C. Stihl, P.V. Vladimirov, Ab initio study of hydrogen diffusion in Be and Be12Ti for fusion applications, Comp Mater Sci 187 (2021) 109921.
[32] M.G. Ganchenkova, P.V. Vladimirov, V.A. Borodin, Vacancies, interstitials and gas atoms in beryllium, J Nucl Mater 386-388 (2009) 79-81.
[33] X.L. Zhu, C.L. Wang, J.J. Liu, X.M. Zhang, H.Q. Deng, W.S. Duan, L. Yang, Retention and diffusion of transmutation H and He atoms in Be12Ti: first-principles calculations, Rsc Adv 8(62) (2018) 35735-35743.
[34] M.L. Jackson, P.A. Burr, R.W. Grimes, Intrinsic defect migration in Be12Ti, Intermetallics 128 (2021) 106937.
[35] Y.L. Wang, C.L. Wang, Z.C. Meng, J.T. Liu, Y.H. Li, L. Yang, Aggregation of retained helium and hydrogen in titanium beryllide Be12Ti: a first-principles study, Rsc Adv 11(55) (2021) 34860-34869.
[36] X.L. Zhu, C.L. Wang, Z.C. Meng, Y.L. Wang, H.Q. Deng, W.S. Duan, L. Yang, First-principles study of hydrogen-vacancy complexes in Be12Ti, J Nucl Mater 525 (2019) 7-13.
[37] L. Messina, Z.W. Chang, P. Olsson, Ab initio modelling of vacancy-solute dragging in dilute irradiated iron-based alloys, Nuclear Instruments & Methods in Physics Research Section B-Beam Interactions with Materials and Atoms 303 (2013) 28-32.
[38] K. Mukai, R. Kasada, J.H. Kim, M. Nakamichi, Electronic descriptors for vacancy formation and hydrogen solution in Be-rich intermetallics, Acta Mater 241 (2022) 118428.
[39] V. Chakin, R. Rolli, R. Gaisin, U. Hoeppener-Kramar, M. Nakamichi, M. Zmitko, Tritium release and retention in beryllium and titanium beryllide after neutron irradiation up to damage doses of 23-38 dpa, Fusion Eng Des 161 (2020) 111938.